Projected changes in the atmospheric dynamics of climate extremes in France

Pascal Yiou, Davide Faranda, Soulivanh Thao, Mathieu Vrac

MDPI

Article

Projected changes in the atmospheric dynamics of climate extremes in France

Pascal Yiou [1], Davide Faranda [1,2,3], Soulivanh Thao [1] and Mathieu Vrac [1]

[1] Laboratoire des Sciences du Climat et de l'Environnement, UMR8212 CEA-CNRS-UVSQ, U Paris-Saclay & IPSL, Gif-sur-Yvette, France
[2] Affiliation 2; e-mail@e-mail.com
* Correspondence: pascal.yiou@lsce.ipsl.fr

Abstract: Extremes of temperature, precipitation and wind have caused damages in France, in the agriculture, transportation and health sectors. Those types of events are largely driven by the atmospheric circulation. The dependence on the global climate change is not always clear, and is the subject of extreme event attribution (EEA). This study reports an analysis of the atmospheric circulation over France for seven events that struck France in the 21st century, in various seasons. We focus on the atmospheric dynamics that leads to those extremes and examine how the probability of atmospheric patterns and their predictability responds to climate change. We analyse how the features of those events evolve in simulations following an SSP585 scenario for future climate. Using a range of CMIP6 simulations helps determining uncertainties linked to climate models.

Keywords: Extreme events; climate change; France

Citation: Yiou, P.; Faranda, D.; Thao, S.; Vrac, M. Title. *Atmosphere* **2021**, *1*, 0. https://doi.org/

Received:
Accepted:
Published:

1. Introduction

Rather than a global perspective, decision makers have emphasized the necessity of projections of regional extremes for adaptation to climate change [1]. Therefore, this paper will focus on a few extreme climate events that recently occurred in continental France. Insurance, health, agriculture and energy sectors (at least in France) are often affected by thermal extremes (cold and hot), extreme precipitation or wind speed. Observations show that the duration of such events rarely exceeds a couple of weeks for a maximum impact. Therefore, the key time scale we will consider in this paper is subseasonal.

A climate or meteorological extreme event is often defined when a key variable (temperature, precipitation, wind speed) exceeds a predefined threshold. This allows computing the probability of the event, and then the change of probability of that event, conditional to a climate change scenario, which is the essence of extreme event attribution (EEA) [2–4]. Many papers of EEA are based on the estimate of probabilities of events, from statistical modeling of exceeding a threshold. This requires tools from extreme value theory (EVT) [5]. The main caveat of some of those studies is that they do not take into account the physical processes leading to the extreme events, like features of the atmospheric circulation. Attempts to connect the atmospheric circulation to variables that define the extremes have been recently devised [6,7]. Shepherd [8] argued that the atmospheric circulation is a key element of the uncertainty in attribution studies. This motivates our focus on features of the atmospheric variability that drive a few key events.

New mathematical tools of extreme event attribution have been recently devised [9]. Those tools focus on *dynamical* properties of the atmospheric circulation. Dynamical properties of physical systems correspond to time derivatives of the variables of the system, which can be determined from well-chosen mathematical and statistical indicators

[10–12]. Faranda *et al.* [10] have argued that such dynamical indicators are related to the predictability of the (atmospheric) system. Hence our paper will deal with estimates of dynamical features linked to the atmospheric predictability. The dynamical indicators we will consider include the local dimension, persistence, and pattern likelihood.

In this paper, we study the atmospheric circulation that prevailed during several extreme climate events that occurred in France since 2000. Our goal is to determine how the atmospheric motion properties can be altered by climate change.

Without being exhaustive, we decided to have a wide panel of types of events. Hence, the events we consider are based on temperature, precipitation or wind speed, and which occurred in the four seasons. In the midlatitudes, those quantities are linked to the large-scale atmospheric circulation [13]. This justifies a focus on the atmospheric dynamics that is related to the considered extremes. Hence, we shall examine how the synoptic scales of the atmosphere that occur during regional temperature, precipitation or wind events can be affected by climate change.

We will determine the values of dynamical indicators of the atmospheric circulation in a reanalysis dataset, for reference extreme events. Then we will assess how those dynamical indicators during those reference events will change, as a response to a future climate scenario (here SSP585). This will be performed by sampling the atmospheric variability due to future climate change from a multi-model ensemble (the Coupled Model Intercomparison Project, phase 6: CMIP6 [14]).

Data and methods will be exposed in Section 2. Results appear in Section 4. Discussion and conclusion appear in Section 5.

2. Materials and Methods

2.1. Observations and reanalyses

We considered the ERA5 reanalysis [15] for the determination of key extreme events since 2000. The ERA5 period is available from 1979 to now, with a horizontal resolution of 0.25°. We computed daily averages for sea-level pressure (SLP), geopotential height at 500hPa (Z500), 2-m temperature (T2m), total precipitation (Pr, which combines rainfall, snowfall and hail), 10-m wind speed and 10-m peak wind speed (W, Wmax). SLP and Z500 fields were extracted for a region covering 80W–30E and 30N–65N. Temperature, precipitation and wind speed fields were extracted over a region covering France (4.5W–8.5E; 42N–51.5N). We then selected the 1018 gridpoints that are included in continental France (excluding Corsica).

2.2. Climate model simulations

We analyze daily output of the Coupled Model Intercomparison Project phase 6 (CMIP6) [14] for 11 historical simulations (see Table 1 for references), and one socio-economic pathway (SSP) scenario [16]. This selection was dictated by the availability of Z500, temperature and precipitation fields on daily time scales at the time of analyses: we have only selected models whose data were fully available for the whole period 1950–2100. The historical simulations cover the period 1950–2014. The forcings are consistent with observations. They include changes in: atmospheric composition due to anthropogenic and volcanic influences, solar forcing, emissions or concentrations of short-lived species and natural and anthropogenic aerosols or their precursors, as well as land use. The SSP585 scenario corresponds to a representative concentration pathway scenario (RCP) with a radiative forcing increase of 8.5 Wm^{-2} in 2100 due to greenhouse gas emissions, relative to pre-industrial conditions [16].

Table 1: List of CMIP6 simulations used in this study, their approximate horizontal resolution and references.

Simulation name	Atmospheric resolution	Data reference
BCC-CSM2-MR	100 km	[17]
CanESM5	500 km	[18]
CNRM-CM6-1-HR	100 km	[19]
CNRM-CM6-1	250 km	[20]
CNRM-ESM2-1	250 km	[21]
INM-CM4-8	100 km	[22]
INM-CM5-0	100 km	[22]
IPSL-CM6A-LR	250 km	[23]
MIROC6	250 km	[24]
MRI-ESM2-0	100 km	[25]
UKESM1-0-LL	250 km	[26]

The simulations of each climate model came in ensembles of several members. For simplicity and because not all ensemble sizes were equal, we picked one member of each model ensemble.

2.3. Bias correction and trend removal

Given that the models have biased representation of the Z500, we apply a statistical bias correction[27] on the Z500 fields allowing to account for climate change [28].

The statistical bias correction method applied is the Cumulative Distribution Function - transform (CDF-t) method, developed by Michelangeli *et al.* [27]. The bias corrections were made through the “CDF-t” R package (available at https://cran.r-project.org/web/packages/CDFt). More theoretical and technical details, as well as first validations and comparisons can be found in [9,28].

This approach links the cumulative distribution function (CDF) of a climate variable (here Z500) from GCM simulations to be corrected, to the CDF of this variable from a reference dataset, here the ERA5 reanalysis dataset [15]. CDF-t can be considered as a variant of the empirical quantile-mapping method but within the appropriate target (here future) time period and therefore accounts for changes of CDF from the calibration period to the projection one.

This bias correction method is applied for each grid-point separately in two different ways. First, CDF-t is applied on a monthly basis to the "raw" ERA5 reanalyses and 11 CMIP6 GCM simulations. The results are called the "non-detrended bias corrections".

Secondly, CDF-t is applied (also on a monthly basis) to ERA5 reanalyses and GCM simulations from which a spatial and seasonal trend is removed. To do so, for each day (in ERA5 and CMIP6), the Z500 spatial average is calculated. Next, for each calendar day (e.g., each January, 1) over the periods of interest (1979–2019 or 2061–2100), a linear fit of the daily Z500 spatial average as a function of time is estimated. This spatial trend is then removed from each Z500 grid-cell value for the specific calendar day. Then the spatial average value estimated for the model during the year 2000 is added to the calendar day. This ensures that a seasonality (estimated for 2000) is preserved, with no trend in the resulting Z500 data. Those seasonally and spatially detrended data are the inputs of CDF-t, providing adjusted values. Hereafter, we refer to those adjusted values as "detrended bias corrections". The removed Z500 spatial average trend corresponds to the spatially uniform shift of Z500, mainly caused by the warming over the region. Hence, by removing this trend, we also removed the first-order thermodynamic effect of warming on Z500 fields. Therefore, the resulting anomalies, which are further bias corrected, indicate changes that are mostly due to dynamical changes of the state of the atmosphere.

CDF-t bias correction can be applied on detrended and non-stationary data [28–32]. Indeed, unlike other bias correction methods that require stationary distributions, the CDF-t approach is explicitly designed to account for changes in the distributions — i.e., to account for non-stationarity — and is thus suited when trends are present in data. This does not imply that CDF-t corrects the trends of the model, but rather that CDF-t mostly preserves the trends from the model data to be corrected.

2.4. Variations of dynamical indicators due to climate change

We extract the daily Z500 fields corresponding to the selected extreme event in the ERA5 reanalysis. We then embed these observed trajectories into historical simulations (1979–2019), and projections (2061–2100) under a high (SSP585) emissions scenarios of the CMIP6 models [14]. This embedding of observed trajectories in climate simulations is performed by looking at best analogues. Using the extreme event attribution vocabulary, we consider the historical simulations (1979–2019) as the *factual* world, i.e. the actual world with the current level of anthropogenic emissions. The SSP585 scenario corresponds to a *counterfactual* world. Contrarily to the traditional counterfactual world representing the world that could have been without climate change, our counterfactual world explores the world that could be under projected trajectories of anthropogenic emissions [2]. This *forward* EEA approach has been used by Van Oldenborgh *et al.* [33], who calculated trends up to 2100 from model outputs, Sweet *et al.* [34] who evaluated the annual maximum storm tide level for four different scenarios of sea level rise (see also Sweet *et al.* [35]) and by Kay *et al.* [36], Yoon *et al.* [37] to project the evolution of fire risks in the future. When we embed the portion of Z500 trajectories corresponding to extreme events, we assume that the circulation patterns associated with the extreme event could be observed in the climate model simulations. This assumption is justified by previous studies where it has been verified that the average analogue distances between observed atmospheric patterns (for Z500 and sea-level pressure) and the Historical model simulations are within the analogue distance of the ERA5 reanalysis [38]. For each extreme event, we follow the approach of Faranda *et al.* [9] by computing the analogs of the observed synoptic patterns in each set of model simulations, and determine their properties. For each daily Z500 field observed during extreme events, we compute the Euclidean distance from all the other daily Z500 fields by a spatial average of grid-point distances and we then select the closest 2% daily Z500 fields. This defines our analogs ensemble. Note that the results do not crucially depend on this percentage provided that it is in the range of 0.5 to 3%. The values of the Euclidean distance allow to determine how well the circulation patterns associated with extreme events fit in the simulations. This metric is what we call "analog quality", defined as the average of the Euclidean distance of the 2% closest fields. In addition, we compute the local dimension d and a persistence θ metrics, which are linked to the predictability of the circulation (see [10,39,40]). We have also checked in a previous study that the dynamical systems metrics found for historical simulations are within one standard deviation of those of the 20CR reanalysis datasets [41]. The local dimension and persistence characterize the recurrences of a system around a state in phase space. In our case, the state is the Z500 map for a given extreme event. Values of d and θ are obtained for every day in the dataset of interest. d provides information on the number of pathways the system can take to reach and leave a state [42,43]. It acts as a proxy for the system's active number of degrees of freedom around the state of interest. $0 < \theta \leq 1$ is a metric of persistence [44] of an atmospheric circulation state in time, i.e. how long the system typically stays around the state of interest. A very persistent state (i.e., with θ^{-1} close to zero) is highly stable (and therefore also highly predictable), while a very unstable state yields $\theta = 1$ and therefore low persistence. The information provided by persistence and predictability are different: persistence is related to very short term predictability, namely the possibility of observing tomorrow a pattern which resembles the one observed today. The the metric

d for Z500 is meant to extend towards subseasonal to seasonal scales, as this metric is linked with the underlying local Lyapunov exponents of the systems [11].

The $d - \theta$ parameters are computed for each selected event, in all models and scenario runs (historical and SSP585), so that we can detect changes in the atmospheric circulation observed during extreme events. A change in the analogs quality tells whether the atmospheric configuration is more or less likely in the historical than in the scenario experiments. A change in the dynamical indices informs on the change of predictability and persistence of the circulation pattern associated with the extreme event.

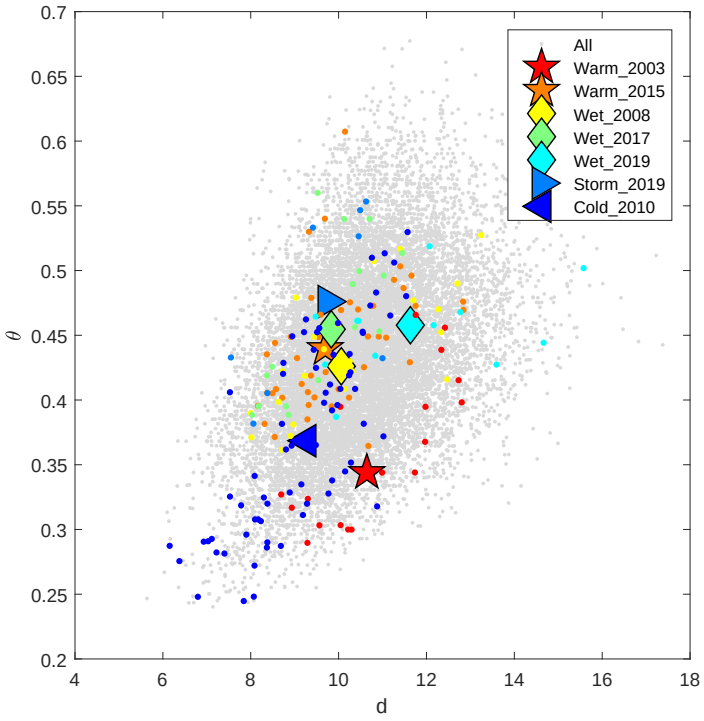

Figure 1. Scatter plot of the daily values of local dimension d and local persistence metric θ determined from the Z500 of the ERA5 reanalysis data. The symbols indicate the median d and θ values for the seven events selected in Sec. 3, stars for heatwaves, diamonds for precipitation events, right triangle for the 2019 storm and left triangle for the 2010 cold spell. The colored dots correspond to daily values of d-θ for each identified event.

3. Selection of events

We decided to chose extreme events that hit France since the beginning of the 21st century. This paper will evaluate how the probability of such events change according to scenarios of climate change, following the approach of Faranda *et al.* [9] that we recalled before.

We determined key years for extremes of temperature, precipitation and wind that occurred in the 21st century. We used a simplified version of the approach of Cattiaux and Ribes [45]. We first considered each season separately (Winter: December-January-February, DJF; Spring: March-April-May, MAM; Summer: June-July-August, JJA; Fall: September-October-November, SON), as the features of extremes depend on the season. For each season and each gridpoint of the ERA5 reanalysis, we determined the 5th (q_{05}) and 95th (q_{95}) quantiles of near-surface temperature (T2m), total precipitation (Pr), wind speed (W) and maximum wind speed (Wmax), between 1979 and 2020. Then for each day t or year y and each gridpoint s, we determine whether the value of climate variable $X \in \{T2m, Pr, W, Wmax\}$ exceeds a 95th quantile threshold. The reason for this

procedure is the high dependence of precipitation and wind speed on altitude: wind speeds exceeding 100 km/h or precipitations rates over 100mm/day are not particularly extreme in mountainous areas, while they are rather rare in plains. Therefore, it is necessary to consider location dependent thresholds (i.e. local quantiles) to detect extremes.

$$\pi(s,t,y) = \begin{cases} 1, & \text{if} X \geq q_{95} \\ 0, & \text{if} X < q_{95}. \end{cases} \quad (1)$$

For each year y, we compute the empirical probability that X exceeds a high threshold (q_{95}) (or is below a low threshold (q_{05})):

$$p(y) = \frac{1}{N_{FR} N_{season}} \sum_{s} \sum_{t \in y} \pi(s,t,y), \quad (2)$$

where N_{FR} is the number of grid point in France ($N_{FR} = 1018$ in ERA5) and N_{season} is the number of days in a season ($N_{seas} \approx 92$). This quantity accounts for the intensity of events (the variable X has to exceed a high threshold), spatial extent (fraction of grid cells for which X exceeds a threshold) and duration (number of days for which X exceeds a threshold).

Figure 2 shows the time series of $p(y)$ for temperature, precipitation and wind speed. The higher values for temperature extremes (Fig. 2a, vertical axis) reflect that thermal events have a larger geographical extent and a longer duration (2–3 weeks). Storms travel across France in a couple of days. Precipitation events generally cover very limited areas and last a couple of days.

In this paper, in order to avoid a tedious exhaustive list of events, we focused on warm winters and summers (which have impacts on human health and ecosystems), cold winters (which have impacts on energy demand and human health), wet springs (that have impacts on agriculture and river management) and falls, and windy winters (due to storms).

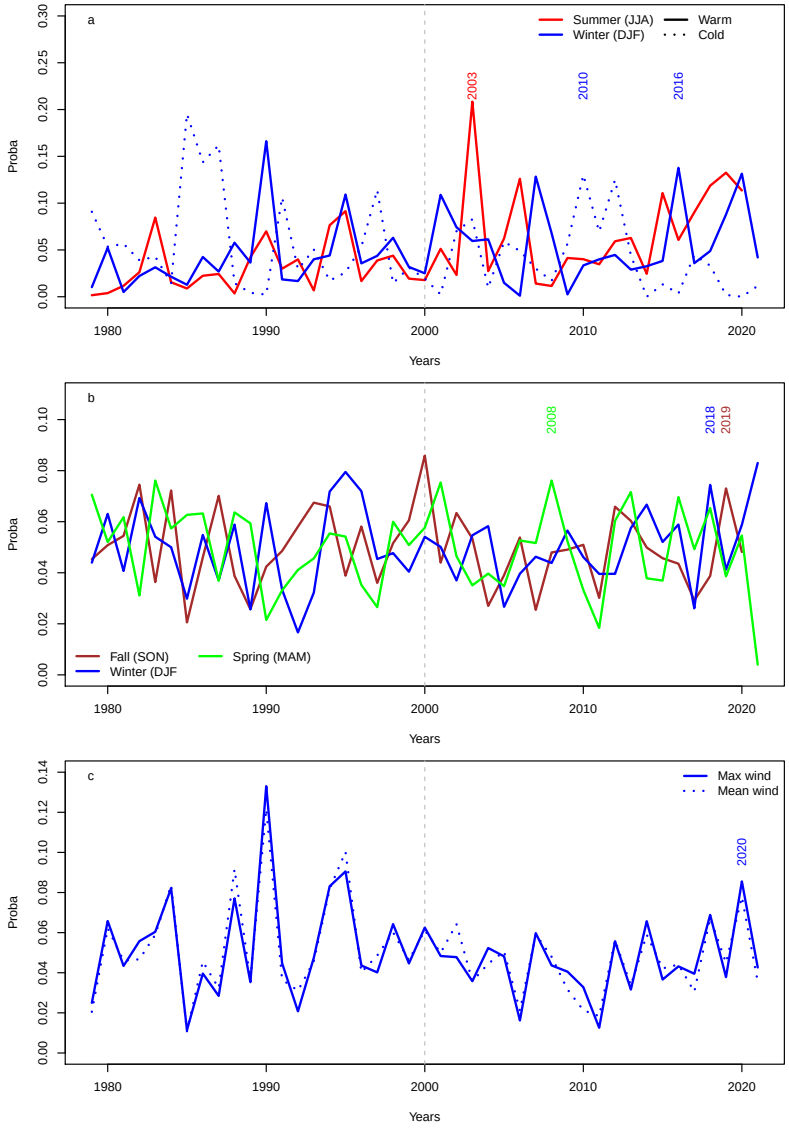

Figure 2. Variations of $p(y)$ for temperature (a), precipitation (b) and wind speed (c). The vertical dashed line is for the year 2000 after which the events are considered. The colors indicate the seasons: red for summer, brown for fall, blue for winter and green for spring. The dotted line in panel (a) indicates the value of p when temperature is below the 5th quantile. The years indicate the records during the 21st century, but excluding 2021.

With this approach, we outline seven remarkable recent years (since 2000), with examples of warm summer (2003) and winter (2016), cold winter (2010), wet spring (2008), wet winter (2018), wet fall (2019), and windy winter (2020). Then we identified event dates from (daily) time series of climate variables. We determined clusters of days when the considered climate variable X exceeds the seasonal average of the 95th quantile of 1018 geographical points (in continental France), with possible excursions below this threshold of no more than 2 days. Shorter "excursion" times to less extreme states (i.e. 1 day or a fully continuous cluster) could have been considered, depending on the impacts of the event. For example, the insurance sector considers that events must be separated by at least 24h to be treated separately. But this only marginally affects the analyses presented in this paper.

The features of those seven identified events are summarized in Table 2.

Table 2: Table of key extreme events in France since 2000. The median local dimension d and persistence metric θ are indicated for each event.

Date of event	Cold	Warm	Wet	Storm	d	θ
31/07/2003 – 17/08/2003		X			0.64	0.34
09/03/2008 – 01/04/2008			X		10.06	0.43
11/12/2009 – 18/02/2010	X				9.27	0.37
01/12/2015 – 13/01/2016		X			9.70	0.44
25/12/2017 – 09/01/2018			X		9.83	0.45
13/10/2019 – 25/10/2019			X		11.63	0.46
06/12/2019 – 15/12/2019			X	X	9.75	0.48

3.1. Summer Heatwaves

The summer 2003 was a heatwave epitome, in term of amplitude and duration [46,47]. This events had huge impacts on the biosphere [48], public health [49] and the economy [REF]. As of 2021, the mean summer temperature of 2003 in France is still the all time record since the beginning of meteorological records.

The mean temperature reached its climax between July 31st and August 17th 2003. The mean seasonal temperature anomalies are shown in Fig. 3 (left). The event was preceded by a drought that started in early May 2003. This prolonged drought hindered latent heat fluxes and hence exacerbated high temperatures. The heat anomaly was also characterized by tropical night time temperatures.

The atmospheric circulation was characterized by a strong anticyclonic pattern centered over France (Fig. 3 (right)), during which almost no wind blew over France, which also enhanced ozone air pollution (and the associated death toll).

The atmospheric circulation of this episode was characterized by a medium local dimension and high persistence (red star in Figure 1).

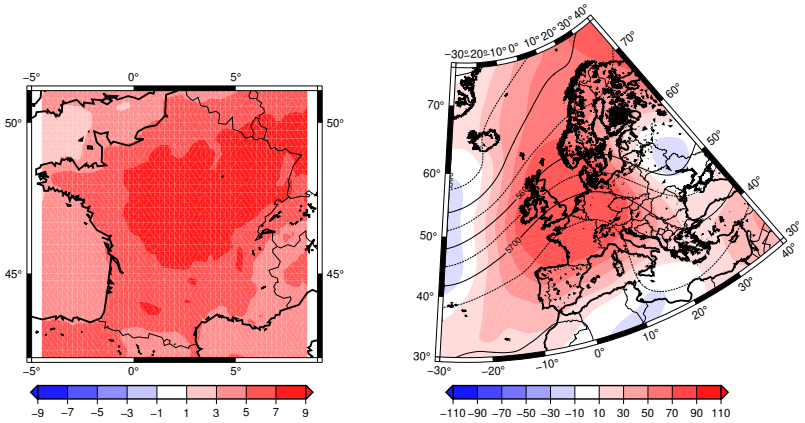

Figure 3. Left panel: mean anomalies of T2m over France between 31/07/2003 and 17/08/2003. Right panel: mean anomalies of Z500 (in m) over the East North Atlantic region (colors). Contour lines indicate the mean Z500 (in m).

3.2. Winter cold spells

The winter of 2009–2010 was exceptionally cold and snowy in Europe and Eastern US [50] (Figure 4 (left)). Although the temperatures were not as cold as historical events such as the winters 1954 or 1963, this cold event created havoc in transportation systems, and was deemed to be the coldest since the beginning of the 21st century.

The atmospheric circulation was cyclonic, with a persisting negative phase of the North Atlantic Oscillation (Figure 4 (right)) [50,51].

The atmospheric circulation of this episode was characterized by a low local dimension and high persistence — low values for θ — (deep blue triangle in Figure 1).

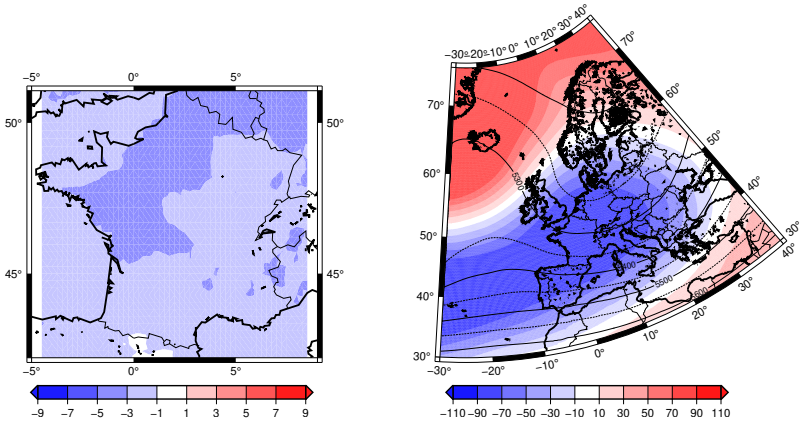

Figure 4. Left panel: mean anomalies of T2m over France between 11/12/2009 and 18/02/2010. Right panel: mean anomalies of (in m) over the East North Atlantic region (colors). Contour lines indicate the mean Z500 (in m).

3.3. Winter warm spells

The winter of 2015–2016 was particularly warm in France (Figure 5 (left)). The previous record of winter temperature occurred in 2006–2007 [52]. This warm spell had a large geographical extent in the northern hemisphere [REF]. In December 2015, no negative temperatures (in Celsius) occurred in France. This had consequences on phenological cycles of plants that require freezing temperatures in order to build defenses against pests [53].

The atmospheric circulation had an anticyclonic pattern over France that extended into North Africa (Figure 5 (right)) [REF]. This warm episode was responsible for air pollution due to atmospheric stagnation [54] in December 2015.

The atmospheric circulation of this episode was characterized by a medium local dimension and low persistence –large values of θ– (orange star in Figure 1).

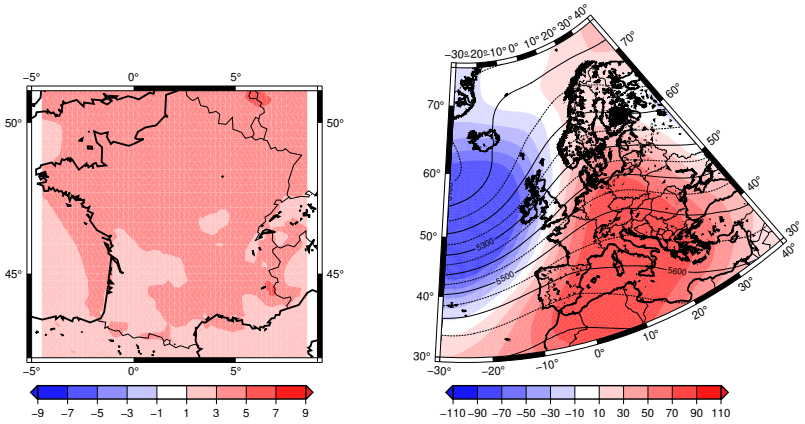

Figure 5. Left panel: mean anomalies of T2m (in K) over France between 01/12/2015 and 13/01/2016. Right panel: mean anomalies of Z500 (in m) over the East North Atlantic region (colors). Contour lines indicate the mean Z500 (in m).

3.4. Wet spring events

Most of March 2008 was rainy. The daily maxima were not exceptional, but the cumulated precipitation flooded northern and central France.

The atmospheric circulation yielded a persisting cyclonic pattern (Fig. 6 (right)) that conveyed moist air into France.

The atmospheric circulation of this episode was characterized by a medium local dimension and medium persistence (yellow diamond in Figure 1).

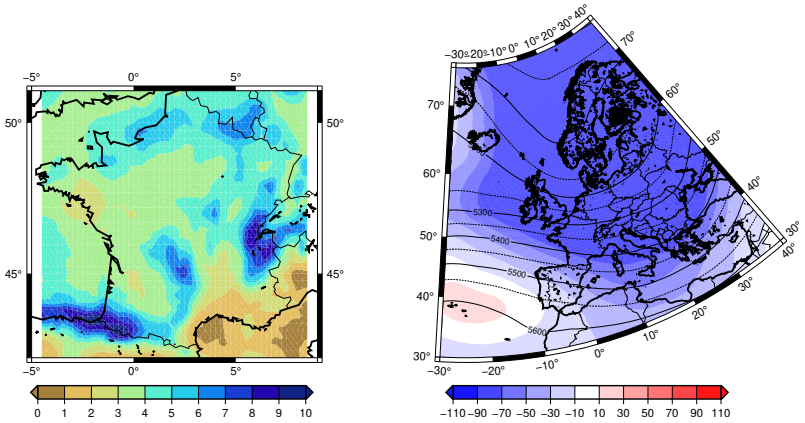

Figure 6. Left panel: mean precipitation rate (in mm/day) over France between 09/03/2008 and 01/04/2008. Right panel: mean anomalies of Z500 (in m) over the East North Atlantic region (colors). Contour lines indicate the mean Z500 (in m).

3.5. Wet winter events

South eastern France witnessed short and intense precipitation at the beginning of December 2017 (storm Ana). The end of December 2017 had a longer spell of precipitation, which hit most of France (Fig. 7 (left)), due to a spate of storms (named Bruno, Dylan, Carmen and Eleanor).

The atmospheric circulation yielded a zonal pattern (Fig. 7 (right)) that brought intense and prolonged precipitations in the southern half of France, along with the storms.

The atmospheric circulation of this episode was characterized by a medium local dimension and medium persistence (green diamond in Figure 1).

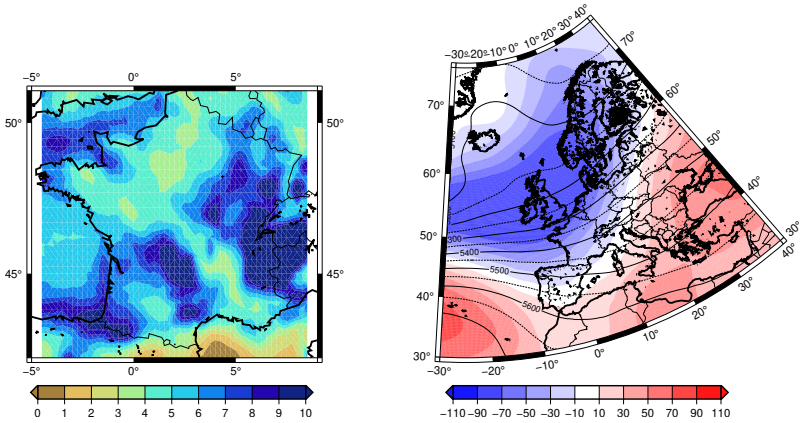

Figure 7. Left panel: mean precipitation rate (in mm/day) over France between 25/12/2017 and 09/01/2018. Right panel: mean anomalies of Z500 (in m) over the East North Atlantic region (colors). Contour lines indicate the mean Z500 (in m).

3.6. Fall Mediterranean events

Mediterranean precipitation events occur in the Fall season over the mountainous regions of the Mediterranean arc, when the Mediterranean sea is still warm and high altitude air has cooled down. Such conditions create strong convective events with devastating effects.

The Fall of 2019 witnessed a large number of Mediterranean events, with a climax in October 2019, during which the Aube region (south east of France) witnessed catastrophic floods that lead to many casualties.

During the October events, the atmospheric circulation had the conjunction of a cyclonic pattern in the eastern North Atlantic and an anticyclonic pattern over central

Europe (Fig. 8 (right)). This meridional circulation pumped moisture into southern France, with a large amount of precipitation during almost two weeks.

The atmospheric circulation of this episode was characterized by a high local dimension and low persistence –high values of θ– (cyan diamond in Figure 1).

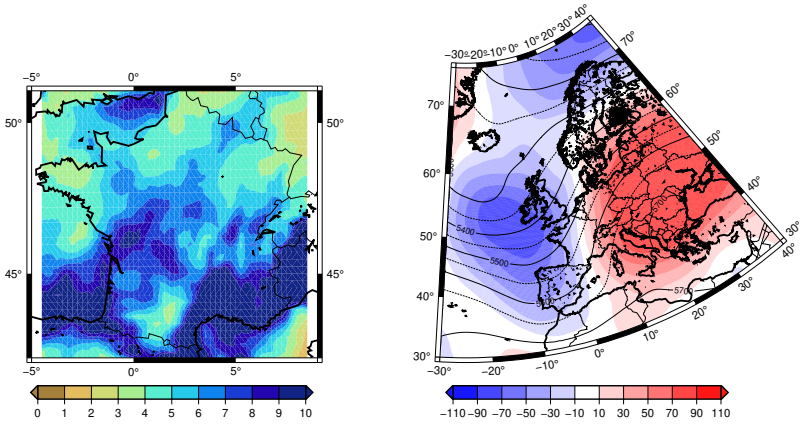

Figure 8. Left panel: mean precipitation rate (in mm/day) over France between 13/10/2019 and 25/10/2019. Right panel: mean anomalies of Z500 (in m) over the East North Atlantic region (colors). Contour lines indicate the mean Z500 (in m).

3.7. Winter storms

Winter North Atlantic storms occur every winter. They start near the Labrador Sea and move across the North Atlantic, following the storm track [55,56]. A few of them can hit France or Europe, especially when the atmospheric circulation is zonal.

The winter of 2019/2020 was particularly stormy, with 10 named storms that hit France between December 2019 and February 2020. Three named storms (Atiyah, Daniel and Elsa) hit France between Dec. 6th and Dec 12th 2019, with wind speeds exceeding 150km/h. During that week, the atmospheric circulation was zonal (Fig. 9 (right)), with cyclonic conditions over Iceland, and anticyclonic conditions near the Azores.

The atmospheric circulation of this episode was characterized by a medium local dimension and low persistence –high values of θ– (light blue triangle in Figure 1).

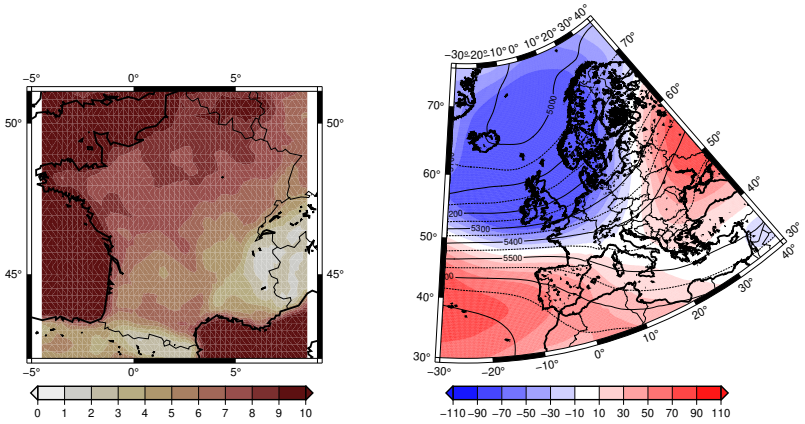

Figure 9. Left panel: mean maximum daily wind speed (in m/s) over France between 06/12/2019 and 15/12/2019. Right panel: mean anomalies of Z500 with respect to the seasonal cycle (in m) over the East North Atlantic region (colors). Contour lines indicate the mean Z500 (in m).

This spate of storms also brought a lot of precipitation over France, and caused local floods.

4. Results

We show how the dynamical features (dimension d– persistence metric θ) of the atmosphere for the seven emblematic events change in scenario simulations.

The present-day values of those dynamical parameters are shown in Figure 1, obtained with the ERA5 reanalysis (1979-2019). We observe that the different events occupy preferential regions of the $d - \theta$ diagram. In particular, the majority of the points for the cold spell of 2010 have high persistence (low θ) and low dimension, which corresponds to the negative phase of the North Atlantic Oscillation [10]. The 2019 wet event occupies a region characterized by blocking patterns. For the other events the identification of the phase space region is not straightforward but one has to keep in mind that in summer the variance of the cloud of points is reduced around the median values. The results discuss the changes of those parameters d–θ for a climate scenario, in CMIP6 simulations.

As discussed in Section 2.3, we determine d–θ for the seven events of the beginning of the 21st century, assuming they occur toward the end of the 21st century. We examine the influence of warming on the dynamical indicators by subtracting the trend in Z500. Hence, the "raw" changes of d–θ indicate, to a first order, a thermodynamical contribution of climate change to the dynamics of the event. The d–θ changes with the "detrended" data corresponds to a change in circulation dynamical features related to predictability.

The results are summarized in Figure 10, which shows how the dynamical features d–θ change (relatively) for each event.

we emphasize that the y-axes are different for panels a) and b). This implies that keeping the trend produces stronger changes in the metrics, with up to 20% of variation (with respect to the historical period) for d, θ in the period 2061-2100 for the circulation associated with the 2003 heatwave. When removing the trends we observe smaller variations of order 2 or 3% for all events. The impact of circulation changes is therefore smaller than the thermodynamical change due to the increase of temperature. In general changes are larger for the end of the century. However we can observe some changes of sign between the two periods for the same metrics.

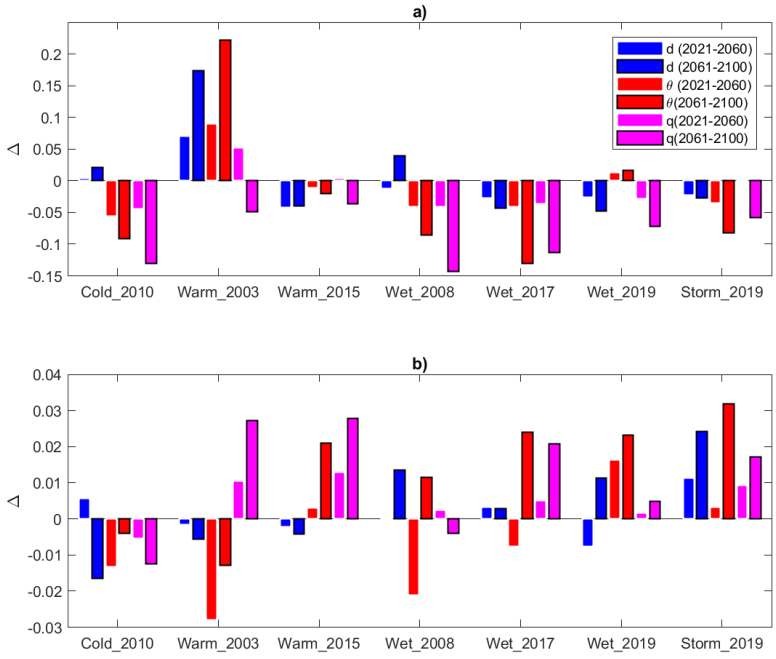

Figure 10. Upper panel (a): d, θ and analog quality (q) changes in the "raw" simulations (Δ values). Lower panel (b): d, θ and analog quality (q) changes in the "detrended" simulations. Each of the seven selected events is represented by six bars. The blue bars are for changes of local dimension d between a reference period 1979–2019 and two SSP585 scenario subperiods (2021–2060 and 2061–2100). The red bars are for changes in persistence *theta*. The purple bars are for changes in the distances of Z500 analogs.

4.1. Circulation for temperature extremes

- Cold Spell 20210. From Fig. 10 we see a modest change in the predictability, the persistence of this event increase in the future (negative variation of θ). The analog quality decreases, meaning that the event is less probable in future climate scenarios, in terms of atmospheric circulation (not just temperature).
- Heatwave 2003. With the trend (Fig. 10a) we have increase of dimension (decrease of predictability) and decrease of persistence and almost zero trends for the analogs quality. We see the impact of removing the trend (Figure 10b). When removing the Z500 trend, the dimension does not change while the persistence increases and the event becomes more probable
- Warm winter 2015. With the Z500 trend this event has almost zero signal in the three metrics (Fig. 10a). When removing the Z500 trend, this event tends to be less persistent and more probable (better analogs quality) in the future (Fig. 10b).

4.2. Circulation for precipitation extremes

- Wet spring 2008 and wet winter 2017. We see no trend in the dimension d. The persistence increases, and the quality of analogs decreases (Fig. 10a). When removing the Z500 trend, we get contrasting signal in the metrics, in particular with better analogs and hence a higher probability of occurrence of the spatial patterns.
- Wet fall 2019. The parameter changes with the "raw" data shows small negative trends in dimension and analogs quality (Fig. 10a). The event become less persistent when removing the Z500 trend, and also more probable with an increased analog quality (Fig. 10b).

4.3. Circulation for a wind extreme

Similarly to the wet (and stormy) winter of 2017, the dynamical metrics changes yield opposite signs for the stormy winter of 2019: the values of dimension and persistence slightly (but consistently) decrease with the thermodynamical effect (due to warming) (Fig. 10b), but the residual signal in dimension and persistence (due to potential pattern changes) increases with a similar amplitude (Fig. 10b). This emphasizes the importance of the dynamical signal (Fig. 10b), with respect to the thermodynamical signal for the genesis of storms. The trends are enhanced between the first subperiod (2021–2060) and the second subperiod (2061–2100) of the CMIP6 SSP585 scenario simulations (blue and red bars in Figure 10).

5. Discussion and conclusion

We illustrate a statistical methodology to assess how the atmospheric circulation properties can change for emblematic recent events that hit France since the beginning of the 21st century, with a multi-model ensemble of climate simulations. This study provides an update of the analyses of Yiou *et al.* [57] and Faranda *et al.* [9] with CMIP6 [14] and ERA5 [15], who essentially used the CMIP5 database [58] and NCEP reanalysis [59] for attribution.

The results were obtained from the physical hypothesis that extreme values of temperature, precipitation or wind speed in France are linked to synoptic atmospheric circulation. This hypothesis is supported by quite a few studies [13,60,61].

The "raw" trends in the dynamical metrics reflect a general increase of the Z500 values (which depends on temperature), so that the quality of analogs seem to increase for the summer, and decrease for the other seasons, as reflected by the theoretical study of Robin *et al.* [62] or the analyses of Vrac *et al.* [63] on seasonal changes of the atmospheric circulation.

Most of the signals conveying dynamical changes are rather small. This is due to the fact that the variability of the atmospheric circulation might be underestimated by climate models [64]. The trends of the dynamics in model simulations can even be opposite to the trend of reanalyses for stormy events [65]. This is the main caveat of our study, which relies on CMIP6 model simulations, whose spatial resolution is on average ten times coarser than the resolution of ERA5. On the other hand, taking a multi-model ensemble allows taking into account implicitly interdecadal variability due to oceans. We find that the changes are almost always amplified with the amplitude of climate change (from 2021–2060 to 2061–2100) when keeping the thermodynamic trend. This enhancement suggests the robustness of the results (which are not obtained "at random"). However, we cannot exclude that interdecadal variability affects the results when removing the trend.

Our results should be interpreted as changes in the likelihood of synoptic circulation (quality of analogs) and predictability of events (d-θ) as a response to climate change, conditional to an emission scenario (SSP585) and a set of climate simulations (from CMIP6). The contrasting signals between the "raw" and "detrended" Z500 in CMIP6 illustrate the relative contributions of thermodynamical and dynamical effects in EEA. The orders of magnitudes are similar to what was found for a specific event (winter 2013/2014) [7,66,67], albeit with other datasets. We observe that the changes of dynamical indicators are rather weak for wet events.

This (admittedly) technical approach to the analysis of extreme events and their relation with the large scale atmospheric circulation is a necessary step for *conditional attribution* (to the atmospheric circulation) of events [4]. We emphasize that this approach is very generic, and could be applied to other events, in other places of the world [e.g. 9,57].

Author Contributions: PY selected the extreme events from ERA5. DF produced the d-θ diagnostics. MV contributed to the bias correction. ST contributed to the dataset management. All authors participated to the writing of the manuscript.

Funding: This research was funded by French ANR project No. ANR-20-CE01-0008 (SAMPRACE), the French Convention de Service Climatique (COSC), and the ERA4CS project EUPHEME.

Data Availability Statement: ERA5 reanalysis data is available from the Copernicus platform (https://climate.copernicus.eu/climate-reanalysis). CMIP6 data (with bias correction) is available on the esgf platform at IPSL (https://esgf-node.ipsl.upmc.fr/).

Acknowledgments: We thank Flavio Pons for his advice on data processing tools.

Conflicts of Interest: The authors declare no conflict of interest. The funders had no role in the design of the study; in the collection, analyses, or interpretation of data; in the writing of the manuscript, or in the decision to publish the results.

Abbreviations

The following abbreviations are used in this manuscript:

CMIP6	Coupled Model Intercomparison Project phase 6
SSP585	Socio-economic Pathway No. 5 with 8.5 W.m^{-2} forcing
Z500	Geopotential height at 500 hPa
SLP	Sea-level pressure
d	Local dimension
θ	Persistence

References

1. Seneviratne, S.; Nicholls, N.; Easterling, D.; Goodess, C.; Kanae, S.; Kossin, J.; Luo, Y.; Marengo, J.; McInnes, K.; Rahimi, M.; Reichstein, M.; Sorteberg, A.; Vera, C.; Zhang, X. Changes in climate extremes and their impacts on the natural physical environment. In *A Special Report of Working Groups I and II of the Intergovernmental Panel on Climate Change (IPCC SREX Report)*; Field, C.; Barros, V.; Stocker, T.; Qin, D.; Dokken, D.; Ebi, K.; Mastrandrea, M.; Mach, K.; Plattner, G.K.; Allen, S.; Tignor, M.; Midgley, P., Eds.; Cambridge University Press: Cambridge, 2012.
2. Jézéquel, A.; Dépoues, V.; Guillemot, H.; Trolliet, M.; Vanderlinden, J.P.; Yiou, P. Behind the veil of extreme event attribution. *Climatic Change* **2018**. doi:https://doi-org.insu.bib.cnrs.fr/10.1007/s10584-018-2252-9.
3. Stott, P.A.; Christidis, N.; Otto, F.E.L.; Sun, Y.; Vanderlinden, J.P.; van Oldenborgh, G.J.; Vautard, R.; von Storch, H.; Walton, P.; Yiou, P.; Zwiers, F.W. Attribution of extreme weather and climate-related events. *Wiley Interdisciplinary Reviews: Climate Change* **2016**, *7*, 23–41. doi:10.1002/wcc.380.
4. National Academies of Sciences Engineering and Medicine., Ed. *Attribution of Extreme Weather Events in the Context of Climate Change*; The National Academies Press: Washington, DC, 2016. doi:10.17226/21852.
5. Coles, S. *An introduction to statistical modeling of extreme values*; Springer series in statistics, Springer: London, New York, 2001.
6. Shepherd, T.G. A Common Framework for Approaches to Extreme Event Attribution. *Current Climate Change Reports* **2016**, *2*, 28–38. doi:10.1007/s40641-016-0033-y.
7. Yiou, P.; Jézéquel, A.; Naveau, P.; Otto, F.E.L.; Vautard, R.; Vrac, M. A statistical framework for conditional extreme event attribution. *Advances in Statistical Climatology, Meteorology and Oceanography* **2017**, *3*, 17–31. doi:10.5194/ascmo-3-17-2017.
8. Shepherd, T.G. Atmospheric circulation as a source of uncertainty in climate change projections. *Nature Geoscience* **2014**, *7*, 703.
9. Faranda, D.; Vrac, M.; Yiou, P.; Jézéquel, A.; Thao, S. Changes in future synoptic circulation patterns: consequences for extreme event attribution. *Geophys. Res. Lett.* **2020**, *47*, e2020GL088002. ISBN: 0094-8276 Publisher: Wiley Online Library.
10. Faranda, D.; Messori, G.; Yiou, P. Dynamical proxies of North Atlantic predictability and extremes. *Scientific reports* **2017**, *7*, 41278.

11. Lucarini, V.; Faranda, D.; Freitas, A.C.M.; Freitas, J.M.; Holland, M.; Kuna, T.; Nicol, M.; Todd, M.; Vaienti, S. *Extremes and recurrence in dynamical systems*; John Wiley & Sons, 2016.
12. Caby, T.; Faranda, D.; Mantica, G.; Vaienti, S.; Yiou, P. Generalized dimensions, large deviations and the distribution of rare events. *Physica D-Nonlinear Phenomena* **2019**. doi: https://doi.org/10.1016/j.physd.2019.06.009.
13. Hurrell, J.; Kushnir, Y.; Ottersen, G.; Visbeck, M., Eds. *The North Atlantic Oscillation : Climatic Significance and Environmental Impact*; Vol. 134, *Geophysical monograph*, American Geophysical Union: Washington, DC, 2003.
14. Eyring, V.; Bony, S.; Meehl, G.A.; Senior, C.A.; Stevens, B.; Stouffer, R.J.; Taylor, K.E. Overview of the Coupled Model Intercomparison Project Phase 6 (CMIP6) experimental design and organization. *Geoscientific Model Development* **2016**, *9*, 1937–1958.
15. Hersbach, H.; Bell, B.; Berrisford, P.; Hirahara, S.; Horányi, A.; Muñoz-Sabater, J.; Nicolas, J.; Peubey, C.; Radu, R.; Schepers, D. The ERA5 global reanalysis. *Quat. J. Roy. Met. Soc.* **2020**, *146*, 1999–2049. ISBN: 0035-9009 Publisher: Wiley Online Library.
16. Riahi, K.; Van Vuuren, D.P.; Kriegler, E.; Edmonds, J.; O'neill, B.C.; Fujimori, S.; Bauer, N.; Calvin, K.; Dellink, R.; Fricko, O. The Shared Socioeconomic Pathways and their energy, land use, and greenhouse gas emissions implications: An overview. *Global environmental change* **2017**, *42*, 153–168. ISBN: 0959-3780 Publisher: Elsevier.
17. Wu, T.; Chu, M.; Dong, M.; Fang, Y.; Jie, W.; Li, J.; Li, W.; Liu, Q.; Shi, X.; Xin, X.; Yan, J.; Zhang, F.; Zhang, J.; Zhang, L.; Zhang, Y. BCC BCC-CSM2MR model output prepared for CMIP6 CMIP piControl, 2018. doi:10.22033/ESGF/CMIP6.3016.
18. Swart, N.C.; Cole, J.N.; Kharin, V.V.; Lazare, M.; Scinocca, J.F.; Gillett, N.P.; Anstey, J.; Arora, V.; Christian, J.R.; Jiao, Y.; Lee, W.G.; Majaess, F.; Saenko, O.A.; Seiler, C.; Seinen, C.; Shao, A.; Solheim, L.; von Salzen, K.; Yang, D.; Winter, B.; Sigmond, M. CCCma CanESM5 model output prepared for CMIP6 ScenarioMIP, 2019. doi:10.22033/ESGF/CMIP6.1317.
19. Voldoire, A. CNRM-CERFACS CNRM-CM6-1-HR model output prepared for CMIP6 HighResMIP, 2019. doi:10.22033/ESGF/CMIP6.1387.
20. Voldoire, A. CNRM-CERFACS CNRM-CM6-1 model output prepared for CMIP6 CMIP, 2018. doi:10.22033/ESGF/CMIP6.1375.
21. Seferian, R. CNRM-CERFACS CNRM-ESM2-1 model output prepared for CMIP6 CMIP, 2018. doi:10.22033/ESGF/CMIP6.1391.
22. Volodin, E.; Mortikov, E.; Gritsun, A.; Lykossov, V.; Galin, V.; Diansky, N.; Gusev, A.; Kostrykin, S.; Iakovlev, N.; Shestakova, A.; Emelina, S. INM INM-CM5-0 model output prepared for CMIP6 CMIP abrupt-4xCO2, 2019. doi:10.22033/ESGF/CMIP6.4932.
23. Boucher, O.; Denvil, S.; Levavasseur, G.; Cozic, A.; Caubel, A.; Foujols, M.A.; Meurdesoif, Y.; Cadule, P.; Devilliers, M.; Ghattas, J.; Lebas, N.; Lurton, T.; Mellul, L.; Musat, I.; Mignot, J.; Cheruy, F. IPSL IPSL-CM6A-LR model output prepared for CMIP6 CMIP, 2018. doi: 10.22033/ESGF/CMIP6.1534.
24. Shiogama, H.; Abe, M.; Tatebe, H. MIROC MIROC6 model output prepared for CMIP6 ScenarioMIP, 2019. doi:10.22033/ESGF/CMIP6.898.
25. Yukimoto, S.; Koshiro, T.; Kawai, H.; Oshima, N.; Yoshida, K.; Urakawa, S.; Tsujino, H.; Deushi, M.; Tanaka, T.; Hosaka, M.; Yoshimura, H.; Shindo, E.; Mizuta, R.; Ishii, M.; Obata, A.; Adachi, Y. MRI MRI-ESM2.0 model output prepared for CMIP6 CMIP, 2019. doi: 10.22033/ESGF/CMIP6.621.
26. Tang, Y.; Rumbold, S.; Ellis, R.; Kelley, D.; Mulcahy, J.; Sellar, A.; Walton, J.; Jones, C. MOHC UKESM1.0-LL model output prepared for CMIP6 CMIP historical, 2019. doi: 10.22033/ESGF/CMIP6.6113.
27. Michelangeli, P.A.; Vrac, M.; Loukos, H. Probabilistic downscaling approaches: Application to wind cumulative distribution functions. *Geophysical Research Letters* **2009**, *36*.
28. Vrac, M.; Drobinski, P.; Merlo, A.; Herrmann, M.; Lavaysse, C.; Li, L.; Somot, S. Dynamical and statistical downscaling of the French Mediterranean climate: uncertainty assessment. *Natural Hazards and Earth System Sciences* **2012**, *12*, 2769–2784. ISBN: 1561-8633 Publisher: Copernicus GmbH.
29. Vigaud, N.; Vrac, M.; Caballero, Y. Probabilistic downscaling of GCM scenarios over southern India. *International journal of climatology* **2013**, *33*, 1248–1263. ISBN: 0899-8418 Publisher: Wiley Online Library.
30. Ayar, P.V.; Vrac, M.; Bastin, S.; Carreau, J.; Déqué, M.; Gallardo, C. Intercomparison of statistical and dynamical downscaling models under the EURO-and MED-CORDEX initiative framework: present climate evaluations. *Climate Dynamics* **2016**, *46*, 1301–1329.

31. Vrac, M.; Noël, T.; Vautard, R. Bias correction of precipitation through Singularity Stochastic Removal: Because occurrences matter. *Journal of Geophysical Research: Atmospheres* **2016**, *121*, 5237–5258.
32. Volosciuk, C.; Maraun, D.; Vrac, M.; Widmann, M. A combined statistical bias correction and stochastic downscaling method for precipitation. *Hydrology and Earth System Sciences* **2017**, *21*, 1693–1719. ISBN: 1027-5606 Publisher: Copernicus GmbH.
33. Van Oldenborgh, G.J.; Van Urk, A.; Allen, M. The absence of a role of climate change in the 2011 Thailand floods. *Bull. Amer. Meteor. Soc* **2012**, *93*, 1047–1049.
34. Sweet, W.; Zervas, C.; Gill, S.; Park, J. Hurricane Sandy inundation probabilities today and tomorrow. *Bulletin of the American Meteorological Society* **2013**, *94*, S17–S20.
35. Sweet, W.V.; Menendez, M.; Genz, A.; Obeysekera, J.; Park, J.; Marra, J.J. In tide's way: Southeast Florida's September 2015 sunny-day flood. *Bulletin of the American Meteorological Society* **2016**, *97*, S25–S30. ISBN: 0003-0007 Publisher: JSTOR.
36. Kay, J.E.; Deser, C.; Phillips, A.; Mai, A.; Hannay, C.; Strand, G.; Arblaster, J.M.; Bates, S.C.; Danabasoglu, G.; Edwards, J. The Community Earth System Model (CESM) large ensemble project: A community resource for studying climate change in the presence of internal climate variability. *Bulletin of the American Meteorological Society* **2015**, *96*, 1333–1349. ISBN: 0003-0007.
37. Yoon, J.H.; Kravitz, B.; Rasch, P.J.; Simon Wang, S.Y.; Gillies, R.R.; Hipps, L. Extreme fire season in California: A glimpse into the future. *Bulletin of the American Meteorological Society* **2015**, *96*, S5–S9. ISBN: 0003-0007 Publisher: American Meteorological Society.
38. Jézéquel, A.; Bevacqua, E.; d'Andrea, F.; Thao, S.; Vautard, R.; Vrac, M.; Yiou, P. Conditional and residual trends of singular hot days in Europe. *Environmental Research Letters* **2020**, *15*, 064018. ISBN: 1748-9326 Publisher: IOP Publishing.
39. Freitas, A.C.M.; Freitas, J.M.; Todd, M. Hitting time statistics and extreme value theory. *Probability Theory and Related Fields* **2010**, *147*, 675–710.
40. Lucarini, V.; Kuna, T.; Wouters, J.; Faranda, D. Relevance of sampling schemes in light of Ruelle's linear response theory. *Nonlinearity* **2012**, *25*, 1311.
41. Rodrigues, D.; Alvarez-Castro, M.C.; Messori, G.; Yiou, P.; Robin, Y.; Faranda, D. Dynamical properties of the North Atlantic atmospheric circulation in the past 150 years in CMIP5 models and the 20CRv2c Reanalysis. *Journal of Climate* **2018**.
42. Liebovitch, L.S.; Toth, T. A fast algorithm to determine fractal dimensions by box counting. *physics Letters A* **1989**, *141*, 386–390. ISBN: 0375-9601 Publisher: Elsevier.
43. Sarkar, N.; Chaudhuri, B.B. An efficient differential box-counting approach to compute fractal dimension of image. *IEEE Transactions on systems, man, and cybernetics* **1994**, *24*, 115–120. ISBN: 0018-9472 Publisher: IEEE.
44. Süveges, M. Likelihood estimation of the extremal index. *Extremes* **2007**, *10*, 41–55. ISBN: 1386-1999 Publisher: Springer.
45. Cattiaux, J.; Ribes, A. Defining single extreme weather events in a climate perspective. *Bulletin of the American Meteorological Society* **2018**, *99*, 1557–1568. doi: https://doi.org/10.1175/BAMS-D-17-0281.1.
46. Schaer, C.; Jendritzky, G. Climate change: Hot news from summer 2003. *Nature* **2004**, *432*, 559–560.
47. Schaer, C.; Vidale, P.; Luthi, D.; Frei, C.; Haberli, C.; Liniger, M.; Appenzeller, C. The role of increasing temperature variability in European summer heatwaves. *Nature* **2004**, *427*, 332–336.
48. Ciais, P.; Reichstein, M.; Viovy, N.; Granier, A.; Ogee, J.; Allard, V.; Aubinet, M.; Buchmann, N.; Bernhofer, C.; Carrara, A.; Chevallier, F.; De Noblet, N.; Friend, A.; Friedlingstein, P.; Grunwald, T.; Heinesch, B.; Keronen, P.; Knohl, A.; Krinner, G.; Loustau, D.; Manca, G.; Matteucci, G.; Miglietta, F.; Ourcival, J.; Papale, D.; Pilegaard, K.; Rambal, S.; Seufert, G.; Soussana, J.; Sanz, M.; Schulze, E.; Vesala, T.; Valentini, R. Europe-wide reduction in primary productivity caused by the heat and drought in 2003. *Nature* **2005**, *437*, 529–533.
49. Vandentorren, S.; Suzan, F.; Medina, S.; Pascal, M.; Maulpoix, A.; Cohen, J.; Ledrans, M. Mortality in 13 French cities during the August 2003 heat wave. *Amer. J. Public Health* **2004**, *94*, 1518–1520.
50. Cattiaux, J.; Vautard, R.; Cassou, C.; Yiou, P.; Masson-Delmotte, V.; Codron, F. Winter 2010 in Europe: A cold extreme in a warming climate. *Geophys. Res. Lett.* **2010**, *37*, doi:10.1029/2010gl044613.

559 51. Sillmann, J.; Croci-Maspoli, M.; Kallache, M.; Katz, R.W. Extreme cold winter temperatures
560 in Europe under the influence of North Atlantic atmospheric blocking. *Journal of Climate*
561 **2011**, *24*, 5899–5913.
562 52. Yiou, P.; Vautard, R.; Naveau, P.; Cassou, C. Inconsistency between atmospheric dynamics
563 and temperatures during the exceptional 2006/2007 fall/winter and recent warming in
564 Europe. *Geophys. Res. Lett.* **2007**, *34*, doi:10.1029/2007GL031981.
565 53. Ben-Ari, T.; Boé, J.; Ciais, P.; Lecerf, R.; Van der Velde, M.; Makowski, D. Causes and
566 implications of the unforeseen 2016 extreme yield loss in the breadbasket of France. *Nature*
567 *communications* **2018**, *9*, 1627. doi:https://doi.org/10.1038/s41467-018-04087-x.
568 54. Vautard, R.; Colette, A.; Van Meijgaard, E.; Meleux, F.; Jan van Oldenborgh, G.; Otto, F.;
569 Tobin, I.; Yiou, P. Attribution of Wintertime Anticyclonic Stagnation Contributing to Air
570 Pollution in Western Europe. *Bulletin of the American Meteorological Society* **2018**, *99*, S70–S75.
571 55. Ulbrich, U.; Leckebusch, G.C.; Pinto, J.G. Extra-tropical cyclones in the present and future
572 climate: a review. *Theoretical and Applied Climatology* **2009**, *96*, 117–131.
573 56. Hoskins, B.J.; James, I.N. *Fluid Dynamics of the Mid-Latitude Atmosphere*; J. Wiley & Sons, 2014.
574 57. Yiou, P.; Cattiaux, J.; Faranda, D.; Kadygrov, N.; Jézéquel, A.; Naveau, P.; Ribes, A.; Robin, Y.;
575 Thao, S.; van Oldenborgh, G.J. Analyses of the Northern European summer heatwave of
576 2018. *Bulletin of the American Meteorological Society* **2020**, *101*, S35–S40.
577 58. Taylor, K.E.; Stouffer, R.J.; Meehl, G.A. An Overview of CMIP5 and the Experiment Design.
578 *Bull. Amer. Met. Soc.* **2012**, *93*, 485–498.
579 59. Kistler, R.; Kalnay, E.; Collins, W.; Saha, S.; White, G.; Woollen, J.; Chelliah, M.; Ebisuzaki,
580 W.; Kanamitsu, M.; Kousky, V.; van den Dool, H.; Jenne, R.; Fiorino, M. The NCEP-NCAR
581 50-year reanalysis: Monthly means CD-ROM and documentation. *Bulletin of the American*
582 *Meteorological Society* **2001**, *82*, 247–267.
583 60. Yiou, P.; Nogaj, M. Extreme climatic events and weather regimes over the North Atlantic:
584 When and where? *Geophys. Res. Lett.* **2004**, *31*, L07202. doi:10.1029/2003GL019119.
585 61. Cassou, C.; Terray, L.; Phillips, A.S. Tropical Atlantic influence on European heat waves.
586 *Journal of Climate* **2005**, *18*, 2805–2811.
587 62. Robin, Y.; Yiou, P.; Naveau, P. Detecting changes in forced climate attractors with Wasserstein
588 distance. *Nonlinear Processes in Geophysics* **2017**, *24*, 393–405.
589 63. Vrac, M.; Ayar, P.V.; Yiou, P. Trends and variability of seasonal weather regimes. *Int. J.*
590 *Climatol.* **2013**, pp. n/a–n/a. doi:10.1002/joc.3700.
591 64. Yiou, P.; Servonnat, J.; Yoshimori, M.; Swingedouw, D.; Khodri, M.; Abe-Ouchi, A. Stability
592 of weather regimes during the last millennium from climate simulations. *Geophysical Research*
593 *Letters* **2012**, *39*. doi:Artn L08703 Doi 10.1029/2012gl051310.
594 65. Vautard, R.; Van Oldenborgh, G.J.; Otto, F.; Yiou, P.; De Vries, H.; Van Mijgaard, E.; Stepek,
595 A.; Soubeyroux, J.M.; Philip, S.; Kew, S. Human influence on European winter wind storms
596 such as those of January 2018. *Earth Systems Dynamic* **2019**, *10*.
597 66. Schaller, N.; Kay, A.L.; Lamb, R.; Massey, N.R.; van Oldenborgh, G.J.; Otto, F.E.L.; Sparrow,
598 S.N.; Vautard, R.; Yiou, P.; Ashpole, I.; Bowery, A.; Crooks, S.M.; Haustein, K.; Huntingford,
599 C.; Ingram, W.J.; Jones, R.G.; Legg, T.; Miller, J.; Skeggs, J.; Wallom, D.; Weisheimer, A.;
600 Wilson, S.; Stott, P.A.; Allen, M.R. Human influence on climate in the 2014 southern England
601 winter floods and their impacts. *Nature Clim. Change* **2016**, *6*, 627–634.
602 67. Vautard, R.; Yiou, P.; Otto, F.; Stott, P.; Christidis, N.; Oldenborgh, G.J.v.; Schaller, N. Attribu-
603 tion of human-induced dynamical and thermodynamical contributions in extreme weather
604 events. *Environmental Research Letters* **2016**, *11*, 114009.